Osmosis-induced hydrodynamic centering of W/O/W double emulsion droplets for quasi-concentric microcapsule/microsphere fabrication

Hao Wu[a, b], Tianyi Jiang[a], Wenlong Wu[a, b], Shanguo Zhang[a], Ming Li[a], Jingzhuo Zhou[b], Mengya Zhu[b], Juzheng Chen[b, c], Ziyong Li[b, c], Yang Lu[c, d], Hongyuan, Jiang[a*]*

[a]School of Mechatronics Engineering, Harbin Institute of Technology, 150001, Harbin, China

[b]Department of Mechanical Engineering, City University of Hong Kong, 999077, Kowloon, Hong Kong SAR, China

[c]Nano-Manufacturing Laboratory (NML), City University of Hong Kong Shenzhen Research Institute, Shenzhen, Guangdong, China 518057.

[d]Department of Mechanical Engineering, The University of Hong Kong, Pokfulam Road, Hong Kong SAR, China

*Corresponding author. Email address: jty_hit@hit.edu.cn, jhy_hit@hit.edu.cn

Abbreviations: water-in-oil-water (W/O/W), trimethoxy(octadecyl)silane (OTS), 2-hydroxy-2-ethylpropiophenone (HMPP), ethoxylate trimethylolpropane triacrylate (ETPTA), poly (vinyl alcohol) (PVA)

Abstract

Water-in-oil-in-water (W/O/W) double emulsion droplets are a typical colloidal system applied in various practical fields. However, certain high-specification applications necessitate exact geometric homogeneity in terms of both shell diameter and thickness. Despite achieving uniformity in shell diameter, on-chip microfluidic emulsification always leads to an eccentric phenomenon due to innate density differences of the droplet solution. At the same time, the current regulation methods have multiple limitations, including their applicability, regulatory scope, and objective restrictions. Herein, we propose an off-chip osmosis-induced hydrodynamic method to accurately regulate the eccentricity of W/O/W double emulsion droplets. The rational selection of hypertonic osmosis can energize the droplets and induce inward transmembrane water flux. This flow helps to reposition the droplet core to align concentrically with the shell, regardless of the initial dimension and eccentricity of the droplets. As the osmotic induction reduces due to the dilution of the inner solute molar concentration, the optimal droplet configuration can be achieved when osmosis-induced hydrodynamic regulation sufficiently counteracts the adverse effects of droplet solution density difference. The microcapsules can thus be produced by instant UV polymerization of the regulated double emulsion droplets, and the silica microspheres with fine geometric homogeneity can be prepared through further heat treatment, which is expected to meet the stringent morphological requirements in practical applications.

Keywords： Microfluidics, W/O/W double emulsion droplet, Osmosis, Hydrodynamic regulation, Microspheres

1. Introduction

Water-in-oil-in-water (W/O/W) double-emulsion droplets are a commonly occurring form of double-emulsion colloidal systems. In this configuration, the dispersed oil globule houses dispersed aqueous compartments and concurrently acts as a protective layer to separate the inner droplets from the continuous aqueous phase [1-3]. To date, W/O/W double emulsion droplets have found promising use in a myriad of practical applications, including pharmaceuticals [4, 5], cosmetics [6, 7], food industry [8, 9], chemical/biomedical analysis [10, 11], material preparation [12, 13], etc., particularly advantageous as microcapsules to encapsulate a variety of hydrophilic active ingredients inside the inner droplets with an extended shelf life [14, 15]. In contrast to conventional microcapsules prepared by spray-drying or single emulsion droplets with interfacial synthetic shells, W/O/W double emulsion droplets possess well-defined shell morphology and dimension, which offers additional benefits to flexibly regulate the release kinetics of the encapsulated substances [16]. However, in order to achieve massive, synchronous controlled release of microcapsules at the

appropriate timing and location, more stringent morphological requirements should be met as a prerequisite. This involves improving the geometric homogeneity of W/O/W double emulsion droplets in terms of both shell diameter and wall thickness. Simultaneously, the use of W/O/W double emulsion droplets also presents similar high-end demands in some specific scenarios related to the preparation of solid microspheres and nanoparticles, such as inertial confinement fusion, high-energy-density physics experiments, high-specification filler manufacturing, and so forth [17-19]. Under these circumstances, meeting the strict standards presents considerable challenges for conventional production methods such as two-stage stirring emulsification and membrane emulsification, particularly when striving to achieve a high level of droplet uniformity [20-22]. In addition, the coaxial electrospray technology can produce submicron-scale droplets through the formation of the Taylor cone. The produced droplets have a relatively fine monodispersity compared to the conventional methods, but the CV value is still insufficient. Furthermore, this technology has a finite selection of available liquid combinations due to limitations in the physical properties of the liquids in light of specific electrical conductivity and viscosity [23]. In recent years, microfluidics has matured and burgeoned into a versatile technical platform to precisely manipulate small volumes of fluids with exquisite composition and morphology [24-28]. The W/O/W double emulsion droplets can be easily prepared by microfluidic emulsification with tailored dimensions, which shall serve as an optimal scheme in terms of droplet size uniformity [29-31]. Nevertheless, the intrinsic density difference between the innermost and outermost globule solutions shall spontaneously induce the shell thickness variation, simultaneously forming thin and thick shell regions on opposite sides, thereby compromising the shell homogeneity. Although numerous investigations have been conducted on the topic of double emulsion droplets [32-35], there are fewer scholars focusing on this eccentricity regulation issue. To circumvent this deficiency, A. Vian [36] prepared W/O/W double emulsion droplets with an ultrathin shell thickness of 800 nm and thus exploited the lubricating effects to inhibit the fluid flow inside the thin shell to obtain better concentricity, but the specialized thin shell condition lacks generality. R. L. Garrell [37] reported an electric field-induced centering method to optimize the shell thickness uniformity. Apart from some basic requirements regarding the electrical properties of the droplets, the density difference of all liquids must be within a tiny range of 0.1%, which can hardly meet the needs of practical applications. Enlightened by the floating phenomenon of long journal bearing, Liang [38] presented a real-time hydrodynamic method to adjust the core-shell double emulsion droplets with fine concentricity by increasing the outer phase flow rate. However, it should be noted that the velocity growth range is relatively finite under the premise of stable droplet generation, and the independent regulation of droplets cannot be realized because the dimension and concentricity are all coupled with the flow rate variation. In

addition, this on-chip dynamic regulation method cannot satisfy the need for off-chip post-processing, since the density difference between the droplet solutions will again dominate and make the droplets eccentric when they are removed from this dynamic generation environment. Osmosis is a thermodynamic behavior in which solvent molecules spontaneously diffuse through a selectively permeable membrane to equalize the solute concentration on both sides, thereby inducing directional fluid motion. [39-43]. As an effective control measure, it has been adopted in various applications, including controlled release [44, 45], acoustic imaging [46, 47], small molecule detection [48, 49], photonic crystal regulation [50, 51], etc. In the case of W/O/W double emulsion droplets, osmosis can energize the droplets and create a hydrodynamic environment through the induced transmembrane water flux. This phenomenon can cause the droplets to either increase or decrease in size, which has been reported to induce controlled coalescence or release in multicore double emulsion droplets [52, 53]. However, there is still a lack of attention given to the eccentricity regulation during the morphological variation of W/O/W double emulsion droplets. This off-chip osmotic regulation can serve as a beneficial addition to on-chip droplet generation, which is expected not only to separate the on-chip simultaneous regulation of droplet dimension and eccentricity by outer phase flow rate adjustment but also to offer ample scope for potential post-processing during the osmotic regulation procedure.

Herein, we reported an osmosis-induced hydrodynamic regulation method to prepare quasi-concentric W/O/W double emulsion droplets. With adequate osmosis induction, the eccentricity of the stably generated double emulsion droplets with the maximum outer phase flow rate could be optimized even further. While the droplets with a relatively higher degree of eccentricity could also benefit from greater osmosis-induced improvement. During the regulation process, the regulatory effect gradually diminished as the inward water flux rate decreased and the density difference gradually became the primary factor causing the droplet to become eccentric once again. Thus, the optimal configuration of the microcapsule could be achieved and locked by UV polymerization of the shell solution during the regulation process, which could be transformed into quasi-concentric silica microspheres through further heat treatment.

2. Experimental Section

2.1. Materials

Surface modification agent trimethoxy(octadecyl)silane (OTS, average Mw=374.67, technical grade), photoinitiator 2-hydroxy-2-methylpropiophenone (HMPP, average Mw=164.20), photosensitive monomer ethoxylate trimethylolpropane triacrylate (ETPTA, average Mw=428), surfactant poly (vinyl alcohol) (PVA, 87~89% hydrolyzed, average Mw=13000-23000), were purchased from Sigma-Aldrich. The silica nanoparticle-loaded xylene solution was provided by

Jingcai Chemical Co. The fluorescent dye Nile red and the organic solvent toluene were supplied by Aladdin. Sodium chloride as the solute to regulate the osmosis magnitude of the inner and outer phase solutions was bought from Tianli Chemical Reagent Co. Ltd. All water used was deionized water prepared with the Millipore Milli-Q system to obtain a resistivity of 18.2 MΩ cm^{-1}. The aqueous inner and outer phase solutions were deionized water stabilized with poly (vinyl alcohol), which accounted for 10% by mass. In addition, several combinations of sodium chloride at different molar concentrations were added to the aqueous inner and outer phase solutions to create osmosis gradients. The oily middle phase solution was the mixture of silica nanoparticle-loaded xylene solution and photosensitive monomer trimethylolpropane ethoxylate triacrylate in a volume ratio of 55:45, in addition to 5% (v/v) photoinitiator 2-hydroxy-2-methylpropiophenone and 1% (v/v) fluorescent pigment particles Nile red, which were uniformly mixed with a magnetic stirrer. The surface modification agent was prepared by dissolving the trimethoxy(octadecyl)silane in the toluene solution in a mass ratio of 1:19. For more information, please refer to our previous report [54].

2.2. Preparation of the glass capillary microfluidic device

As shown in Figure 1a, the W1/O/W2 double emulsion droplets were generated using a delicate microfluidic device consisting of two cylindrical glass capillary tubes (1B100-6, World Precision Instruments, Inc., outer diameter 1.03 mm) and one square glass tube (810-9917, AIT Glass, Inc., inner diameter 1.05 mm). The specific fabrication process of the microfluidic device could be divided into two steps, including the pretreatment of the glass capillary tubes and the subsequent sequential assembly as listed below.

2.2.1 Pretreatment of glass capillary tubes

The pretreatment of glass capillary tubes mainly consisted of two aspects: first, the preparation of the tube tip and the corresponding dimensional adjustment. Second, wettability control by surface chemical modification. In the first step, the cylindrical glass capillary tube was first fixed on a micropipette puller (P-97, Sutter Instrument, Inc.), and then the middle part of the tube was subjected to simultaneous heating and bidirectional pulling motion, where the tube broke into two cylindrical glass tubes with identical sharp closed conical tips at one end. The newly formed cylindrical glass capillary tubes were then transferred to a microforge (MF-900, Narishige, Tritech Research, Inc.) to adjust the aperture size to 45 μm and 250 μm, respectively. This was accomplished by first selecting the appropriate location in the horizon of an optical microscope, followed by flash heating to fuse and break the glass at the prescribed location. Finally, the openings of the cylindrical glass capillary tubes were smoothed with sandpaper and cleaned for further processing.

To ensure the stable flow of the oily middle phase solution, its flow path, including the outer wall of the cylindrical glass tube with the smaller aperture and the inner wall of the square glass tube on the same side, inside the microfluidic device had to be chemically treated to be hydrophobic. Among them, the treatment method for the outer wall of the cylindrical glass capillary tube was realized by first immersing the internally ventilated cylindrical glass capillary tube in the prepared surface modification agent for thirty seconds, and then transferring the glass tube to a hot plate for baking to evaporate the toluene, thus coating the precipitated solute trimethoxy(octadecyl)silane on the outer wall surface. Similarly, the inner wall of the square glass tube was treated by controlling the injection pressure of a syringe so that the surface modification agent infiltrated the designated area for 30 seconds, followed by an analogous heating and baking process. As a result, the transparency of the treated glass surfaces was obviously reduced.

2.2.2 Assembly of glass capillary tubes.

The assembly of glass capillary tubes started with fixing the square glass tube on a rectangular glass slide with epoxy adhesive while making sure that the edge of the square glass tube was parallel to that of the glass slide. Then, the glass slide was fixed with tapes on an optical microscope and the subsequent manipulation was observed through the lens to improve the assembly accuracy to the micrometer level. The two cylindrical capillary glass tubes were then inserted from the two opposite ends of the square glass tube, manually aligned coaxially, and fixed to ensure a distance of 220 μm. The co-axiality of the two cylindrical glass capillary tubes was confirmed by checking whether the image clarity of the two cylindrical capillary glass tubes in the microscopic view changed simultaneously when the focal length of the microscope was continuously adjusted. Thus, the microfluidic device adopted a flow-focusing configuration in which the inner and middle phase solutions flowed individually through the cylindrical tube and the assembled space between the cylindrical and square tubes on the left side, while the outer phase solution and the as-prepared W1/O/W2 double emulsion droplets were arranged on the right side, as shown in Figure 1a. The newly assembled microfluidic device should be left overnight to allow the adhesive to dry, followed by repeated rinses with alcohol and deionized water to remove any dust and contaminants before use. More details can be found in our previous reports [55].

2.3. Experimental setup and manipulation

The preparation of W1/O/W2 double emulsion droplets was performed in a homemade microfluidic device, in which each phase solution was first loaded into glass syringes (Hamilton) and then mounted on three syringe pumps (Harvard Apparatus). Teflon tubes were used to connect the glass syringes loaded with different solutions to the corresponding inlets of the microfluidic

device. This allowed the flow rate of each phase solution to be digitally controlled with high precision. During the manipulation process, the syringe pump loaded with the outer phase solution was first activated with an initial flow rate of 10 ml/h. Until the outer phase solution filled the whole microfluidic device, the second syringe pump loaded with the middle phase solution started working and was gradually adjusted to form stable oil-in-water single emulsion droplets (Here, the ultimate flow rate of the middle phase solution during the experiment was 1 ml/h). Then, the last syringe pump was started, and the corresponding flow rate of the inner phase solution was continuously adjusted to make the three-phase solutions encountered at the gap between the two cylindrical capillary glass tubes and underwent one-step successful emulsification in a dripping regime to obtain the final core-shell structure (Here, the ultimate flow rate of the inner phase solution during the experiment was 2 ml/h). Finally, W1/O/W2 double emulsion droplets with different dimensions and eccentricities were obtained by constantly adjusting the flow rate of the outer phase solution while keeping the flow rates of the other two-phase solutions constant. The corresponding as-prepared double emulsion droplets were then collected in vials for observation and further processing.

2.4. Characterization

The optical and corresponding fluorescent images of the W1/O/W2 double emulsion droplets were monitored with an optical microscope system (BX53, Olympus) equipped with a high-speed digital CCD camera (DP27, Olympus). The SEM images of the quasi-concentric microcapsule and the derived silica microspheres were taken with a scanning electron microscope (SU8010, Hitachi), in which some silica microspheres were intentionally damaged to reveal the wall thickness within the fracture area. In addition, the EDS elemental analysis result of the quasi-concentric microsphere was analyzed by the energy dispersive spectrometer attached to the scanning electron microscope. The thermogravimetric profile of the polymer microcapsule was characterized by a simultaneous thermal analyzer (STA449F3, NETZSCH) at a ramp rate of 10 °C min^{-1} from ambient temperature to 800 °C. During the heat treatment experiments, an electric furnace (QSH-1700-2020T, Quanshuo Electric Furnace Co. Ltd.) was used to perform the debinding and sintering process in the air

3. Results and discussion

3.1 Microfluidic fabrication and characterization of W1/O/W2 double emulsion droplets

As shown in Figure 1a, the W1/O/W2 double emulsion droplets were prepared through a direct one-step microfluidic emulsification process with an appropriate combination of three-phase flow rates. To investigate the effect of solution density difference on the morphology transition of double emulsion droplets in a static environment, a control group was created by allowing the same batch

of as-prepared droplets to stand freely for a certain period of time, as illustrated in Figures 1b and 1c. For quantitative statistical analysis, the eccentricity (ε) of double emulsion droplets was defined as the ratio of the deviation between two centers to the deviation in radii of the innermost and outermost globules. The comparison results revealed that the double emulsion droplets exhibited well monodispersity with a small range distribution in the shell diameter. Nonetheless, the eccentricity of double emulsion droplets changed from a wide scope distribution with a concentrated range between 0.1 to 0.5 to completely eccentric, where all droplets possessed an eccentricity greater than 0.6. This demonstrated that the solution density difference could indeed act as an adverse dominant factor, which spontaneously led to the eccentricity phenomenon and jeopardized the shell thickness homogeneity of double emulsion droplets. Furthermore, to analyze the effect of solution density difference on the morphological variation of double emulsion droplets in the on-chip hydrodynamic environment, a series of double emulsion droplets were generated with gradients of outer phase flow rate as depicted in Figure 2. It could be derived that a stable dripping regime was maintained in the droplet generation process, resulting in double emulsion droplets that displayed fine monodispersity when the outer phase flow rate was 25 ml/h or lower. Moreover, the shell diameter and eccentricity of double emulsion droplets varied synchronously and showed an inverse relationship with respect to the increment of the outer phase flow rate, where the minimum value of the droplet eccentricity could reach around 0.15. Simultaneously, the negative impact of the solution density difference gradually decreased, which was compensated by the ongoing improvement in hydrodynamic regulation performance. When the outer phase flow rate was further increased to 30 ml/h, the droplet generation process shifted from dripping to jetting mode, in which the liquid jets were dragged further and eventually broke up due to the Rayleigh instability [56, 57]. This led to the formation of polydispersed droplets with multiple shell diameters as shown in Figure 2f. Therefore, the regulation range of this on-chip hydrodynamic method by altering the outer phase flow rate was limited and there was still room for further improvement in terms of the eccentricity of double emulsion droplets.

3.2 Osmosis-induced hydrodynamic regulation of W1/O/W2 double emulsion droplets

To overcome the limitations of the on-chip hydrodynamic regulation technique, we employed hypertonic osmosis to energize the droplet. This was accomplished by adding a higher molar concentration of sodium chloride to the aqueous inner phase solution (W1). Consequently, a dynamic inward flux of water was induced even in the off-chip environment. Firstly, it was imperative to investigate whether osmosis-induced hydrodynamic regulation could further optimize the eccentricity of double emulsion droplets, even those generated with the previously maximum outer phase flow rate of 25 ml/h. Additionally, it was necessary to clarify the influence of osmosis

magnitude as well. Therefore, four combinations of osmotic gradients were prepared by varying the molar concentration of sodium chloride in the W2 solutions (ranging from 0.1 mol/L to 0.8 mol/L), while the W1 solution was kept constant at 0.8 mol/L. Then, the prepared samples were incubated for further analysis and the results were exhibited in Figure 3. It was found that three batches of double emulsion droplets with a higher osmotic magnitude of the W1 solution showed an increase in shell diameter. This resulted from the inward transmembrane water transport process, which was positively correlated with the difference in solute molar concentration. While the shell diameter of the isotonic double emulsion droplets decreased slightly due to the evaporation of volatiles such as xylene in the shell solution. Since the evaporation volume was limited, as indicated by the finite reduction of the droplet shell diameter, its effect on the variation of droplet eccentricity was anticipated to be disregarded. Furthermore, there was a notable correlation between the degree of osmosis and the variation in eccentricity of double emulsion droplets. Despite all droplets ultimately becoming eccentric, the osmosis-induced hydrodynamic regulation played a crucial role in the early stages, with its performance in regulation being proportional to the deviation in solute molar concentration, and the maximum osmotic difference could further reduce the eccentricity of double emulsion droplets produced with the maximum outer phase flow rate to below 0.1, as indicated by the pink triangle in Figure 3b. While the other two hypertonic double emulsion droplets can barely refine the droplet eccentricity as the comparatively weaker osmosis-induced hydrodynamic regulation could only partially counteract the negative effects derived from the droplet solution density difference, and afterward became eccentric as the isotonic droplets did. In addition, it was worth noting that although the osmosis-induced hydrodynamic regulation attenuated over time in all hypertonic double emulsion droplets, the slope of their corresponding eccentricity curve varied significantly, with the smallest hypertonic double emulsion droplets, denoted by the red circle, exhibited a similar slope in the eccentricity curve to that of the isotonic droplet, indicating that the influence of the difference in solution density of the droplets outweighed the effect of the small osmotic regulation, rendering it negligible in a later time. In the case of double emulsion droplets with a relatively larger hypertonic difference, the effect of osmosis-induced hydrodynamic regulation could persist for a longer period, culminating in a reduced eccentricity slope. Hence, the osmosis-induced hydrodynamic regulation process could be divided into two stages, as shown in Figure 3c. In the first stage, greater osmotic induction chemically led to larger inward water flux, and the effect of osmosis-induced hydrodynamic regulation dominated over the negative effect derived from the droplet solution density difference. Due to the physical eccentricity of the droplet, water discharge was much higher in the thin-walled region, as it had a shorter transportation distance. Conversely, the thick-walled region reduced the water transportation efficiency, resulting in a slower

flow rate for water transmembrane movement. This velocity difference in water transportation could thus induce directional water movement within the droplet core in accordance with the reduction gradient of water transport velocity, which further enabled the droplet core to reposition and align concentrically with the shell. In the second stage, the osmosis-induced hydrodynamic regulation performance decreased as the osmosis magnitude declined along with the dilution of the solute molar concentration, causing a decrease in the inward water flux rate. Due to a shift in the dominant factor to the droplet solution density difference, the droplet gradually became eccentric. Thus, the optimal configuration of double emulsion droplets having a fine concentricity could be achieved at the end of the first stage and the beginning of the second stage of this off-chip osmotic regulation process.

Subsequently, to further confirm the feasibility of this method, we increased the sodium chloride molar concentration of the W1 solution to 2 mol/L and created a stronger hypertonic environment. This was done to verify the effect of osmosis-induced hydrodynamic regulation on larger droplets with a higher initial eccentricity. Figure 4(a-f) displayed optical and fluorescent images of double emulsion droplets captured at different time points during the osmosis-induced hydrodynamic regulation process from the beginning to the occurrence of ultimate droplet rupture. This rupture phenomenon should be attributed to the interfacial instability caused by the volatile evaporation and the droplet solution density difference. The corresponding statistical results of the droplets' shell diameter and eccentricity were presented in Figures 4g and 4h and the variation trend was found to be similar to the previous observation for the hypertonic droplet with the largest osmotic magnitude in Figure 3b. Nevertheless, some discrepancies remained. The droplet shell diameter and eccentricity underwent significant changes resulting from a stronger osmotic induction. The variation rate for both droplet shell diameter and eccentricity increased concurrently. In this osmosis-induced hydrodynamic regulation process, the minimum value of droplet eccentricity was reduced to less than 0.1. Although the rate of variation near the minimum value was smaller compared to both ends, it was still substantially larger than the smaller osmotic induction group's counterpart as shown in Figure 3. This could be ascribed to the strengthening interaction between the osmotic induction and the droplet solution density difference. Increasing solute concentration was a double-edged sword, not only enhancing the performance of osmotic induction but also expanding the droplet solution density difference. Therefore, if the droplet eccentricity was regulated by a much higher osmotic induction, it was critical to secure the optimal configuration as soon as possible because the quasi-concentric droplet could quickly become eccentric when the much higher droplet solution density difference dominated the interaction process.

3.3 Quasi-concentric microcapsule/microsphere fabrication based on osmosis-induced

hydrodynamic regulation of W1/O/W2 double emulsion droplets

In order to attain fine geometric homogeneity in microcapsules and microspheres suitable for high-specification standards necessary for practical applications, an ingenious technical process was proposed as shown in Figure 5a. Firstly, the microfluidic generated W1/O/W2 double emulsion droplets served as the soft templates and thus were incubated for osmosis-induced hydrodynamic regulation to search for the best concentric configuration. Secondly, the optimal configuration of W1/O/W2 double emulsion droplets was locked through instant UV polymerization of the photosensitive monomer ETPTA in the shell solution. This process also led to the formation of the polymer microcapsules as shown in the inset SEM image, which corresponded to the optimal droplet configuration marked by the pink triangle in Figure 3b. Meanwhile, the cross-linked ETPTA polymer network encapsulated the silica nanoparticles originally dissolved in the xylene solution. Thirdly, a heat treatment process was implemented, which further transformed the polymer microcapsules into quasi-concentric silica microspheres. In the third step, the heat treatment parameters were predetermined based on the results of the thermogravimetric analysis of the solidified shell solution. Figure 5b showed a significant mass loss between approximately 250°C to 500°C. Therefore, the first main stage of debinding in the heat treatment process was set from 200°C to 550°C with a slow ramping velocity of 2 °C/min, followed by a 2-hour preservation time to fully eliminate the organic substances. As shown in Figure 5c, the second main stage of sintering in the heat treatment process continued to ramp up to 1200°C and was maintained for 2 hours to transform discrete nanoparticles into smooth thin walls. The morphology of a large number of thin-walled microspheres could be clearly identified in Figures 5d and 5e. They inherited the fine shell diameter homogeneity from the microfluidics. From the results of the EDS elemental analysis in Figure 5f, the Si and O elements were evenly dispersed, which verified the feasibility of this technical route. In addition, it was worth noting that quasi-concentric ceramic microspheres could be prepared with other materials by simply replacing the input particles. For example, uranium dioxide powder could be used for the preparation of kernel particle in high-temperature gas-cooled fission reactors while granular borosilicate can be utilized for the fabrication of high-quality syntactic foam fillers, thus demonstrating the versatility of this technique. Finally, the eccentricity of the silica microspheres before and after osmosis-induced hydrodynamic regulation, which corresponded to the pink triangle in Figure 3b, was confirmed by observing the artificially crushed microspheres as shown in Figures 5g and 5h, respectively. The wall thickness of osmotically regulated microspheres was uniformly similar at the crack depicted in Figure 5g. In contrast, those that lack regulation displayed notable thickness discrepancies, with the thicker portion being roughly four times the thinner counterpart, as indicated by the white size markings in Figure 5h. As a result, this study validated that combining

on-chip microfluidic generation of W/O/W double emulsion droplets with off-chip osmosis-induced hydrodynamic regulation was a promising and effective approach to fabricating microcapsules/microspheres with better geometric homogeneity in both shell diameter and wall thickness. The prepared microcapsules/microspheres were then expected to fulfill the geometric requirements of specific applications that demanded strict geometric specifications.

3. Conclusion

In this study, we proposed an off-chip osmosis-induced hydrodynamic method for accurately regulating the eccentricity of W/O/W double emulsion droplets produced by on-chip microfluidic emulsification. The regulation process revealed that osmotic induction was not only appropriate for regulating droplets of varying dimensions and eccentricities but could also further break through the limitations of the on-chip hydrodynamic regulation method. During incubation, the osmotic induction magnitude reduced as the inner solute molar concentration was diluted. Consequently, the optimal droplet configuration was attained when osmosis-induced hydrodynamic regulation was just enough to counteract the adverse effects of droplet solution density difference. Furthermore, it was crucial to solidify the droplet's optimal configuration as soon as possible when a potent osmotic induction was applied because the droplet could quickly become eccentric due to the dominant effect of the much higher droplet solution density difference. The regulated droplets could then function as soft templates for producing microcapsules or microspheres through instant UV polymerization and subsequent heat treatment. The high geometric homogeneity of the resulting silica microspheres was validated by SEM analysis, which was expected to meet the stringent morphological requirements in practical applications.

CrediT authorship Contribution statement

This paper was written through the contributions of all authors and the specific contributions were listed as follows: conceptualization, methodology, investigation, experimentation, original drafting (H.W.); supervision, revision, and editing, resources, project administrator (T.J); investigation, resources (W.W); investigation (S.Z); investigation (M.L); resources (J.Z); investigation (M.Z); methodology, investigation (J.C); investigation (Z.L); visualization, supervision, funding acquisition (Y.L); supervision, funding acquisition, resources (H.J). All authors have approved the final version of the manuscript.

Declaration of competing interest

The authors declare no conflict of interest.

Data availability

Data will be made available upon reasonable request.

Acknowledgments

This work is financially supported by the National Natural Science Foundation of China (No.11872165), the Science & Technology Department of Sichuan Province under the grant 2022YFSY0001, and the grant from "Innovation and Technology Fund (ITF) project (GHP/221/21GD).

Appendix A. Supporting information

Supplementary data associated with this article can be found in the online version.

References

[1] N. Garti, C. Bisperink, Double emulsions: Progress and applications, Current Opinion in Colloid & Interface Science, 3 (1998) 657-667, https://doi.org/10.1016/s1359-0294(98)80096-4.

[2] E. Kwak, J. Lee, Y.-J. Jo, M.-J. Choi, Effect of electrolytes in the water phase on the stability of W1/O/W2 double emulsions, Colloids and Surfaces A: Physicochemical and Engineering Aspects, 650 (2022) 129471, https://doi.org/10.1016/j.colsurfa.2022.129471.

[3] C. Zhou, P. Zhu, X. Han, R. Shi, Y. Tian, L. Wang, Microfluidic generation of ATPS droplets by transient double emulsion technique, Lab Chip, 21 (2021) 2684-2690, https://doi.org/10.1039/d1lc00351h.

[4] C.E. Mora-Huertas, H. Fessi, A. Elaissari, Polymer-based nanocapsules for drug delivery, Int. J. Pharm., 385 (2010) 113-142, https://doi.org/10.1016/j.ijpharm.2009.10.018.

[5] H. Zhang, W. Cui, X. Qu, H. Wu, L. Qu, X. Zhang, E. Makila, J. Salonen, Y. Zhu, Z. Yang, D. Chen, H.A. Santos, M. Hai, D.A. Weitz, Photothermal-responsive nanosized hybrid polymersome as versatile therapeutics codelivery nanovehicle for effective tumor suppression, Proc Natl Acad Sci U S A, 116 (2019) 7744-7749, https://doi.org/10.1073/pnas.1817251116.

[6] M. Jacquemond, N. Jeckelmann, L. Ouali, O.P. Haefliger, Perfume-containing polyurea microcapsules with undetectable levels of free isocyanates, J. Appl. Polym. Sci., 114 (2009) 3074-3080, https://doi.org/10.1002/app.30857.

[7] C. Perez, I.J. Castellanos, H.R. Costantino, W. Al-Azzam, K. Griebenow, Recent trends in stabilizing protein structure upon encapsulation and release from bioerodible polymers, J. Pharm. Pharmacol., 54 (2002) 301-313, https://doi.org/10.1211/0022357021778448.

[8] A. Downham, P. Collins, Colouring our foods in the last and next millennium, International Journal of Food Science & Technology, 35 (2000) 5-22, https://doi.org/10.1046/j.1365-2621.2000.00373.x.

[9] X. Chen, D.J. McClements, J. Wang, L. Zou, S. Deng, W. Liu, C. Yan, Y. Zhu, C. Cheng, C. Liu, Coencapsulation of (-)-Epigallocatechin-3-gallate and Quercetin in Particle-Stabilized W/O/W Emulsion Gels: Controlled Release and Bioaccessibility, J. Agric. Food. Chem., 66 (2018) 3691-3699, https://doi.org/10.1021/acs.jafc.7b05161.

[10] X. Chen, L. Hou, Z. Yin, K. Wang, Z. Zhang, F. Bao, NIR light-triggered core-coalescence of double-emulsion drops for micro-reactions, Chem. Eng. J., 454 (2023) 140050, https://doi.org/10.1016/j.cej.2022.140050.

[11] Y. Jia, Y. Ren, W. Liu, L. Hou, Y. Tao, Q. Hu, H. Jiang, Electrocoalescence of paired droplets

encapsulated in double-emulsion drops, Lab Chip, 16 (2016) 4313-4318, https://doi.org/10.1039/c6lc01052k.
[12] H. Wu, Y. Ren, L. Hou, T. Jiang, H. Jiang, Fabrication of syntactic foam fillers via manipulation of on-chip quasi concentric nanoparticle-shelled droplet templates, Lab Chip, 20 (2020) 4600-4610, https://doi.org/10.1039/d0lc00730g.
[13] I. Kimura, T. Sekine, Y. Endo, Production of calcium magnesium phosphate microspheres in a water-in-oil-in-water dispersion, Colloids and Surfaces A: Physicochemical and Engineering Aspects, 613 (2021) 126089, https://doi.org/10.1016/j.colsurfa.2020.126089.
[14] C.H. Choi, H. Wang, H. Lee, J.H. Kim, L. Zhang, A. Mao, D.J. Mooney, D.A. Weitz, One-step generation of cell-laden microgels using double emulsion drops with a sacrificial ultra-thin oil shell, Lab Chip, 16 (2016) 1549-1555, https://doi.org/10.1039/c6lc00261g.
[15] S.H. Kim, J.W. Kim, J.C. Cho, D.A. Weitz, Double-emulsion drops with ultra-thin shells for capsule templates, Lab Chip, 11 (2011) 3162-3166, https://doi.org/10.1039/c1lc20434c.
[16] L. Shang, Y. Cheng, Y. Zhao, Emerging Droplet Microfluidics, Chem. Rev., 117 (2017) 7964-8040, https://doi.org/10.1021/acs.chemrev.6b00848.
[17] D.T. Goodin, N.B. Alexander, G.E. Besenbruch, A.S. Bozek, L.C. Brown, L.C. Carlson, G.W. Flint, P. Goodman, J.D. Kilkenny, W. Maksaereekul, B.W. McQuillan, A. Nikroo, R.R. Paguio, R.W. Petzoldt, R. Raffray, D.G. Schroen, J.D. Sheliak, J. Spalding, J.E. Streit, M.S. Tillack, B.A. Vermillion, Developing a commercial production process for 500 000 targets per day: A key challenge for inertial fusion energy, Physics of Plasmas, 13 (2006) 056305, https://doi.org/10.1063/1.2177129.
[18] H. Wu, J. Chen, K. Duan, M. Zhu, Y. Hou, J. Zhou, Y. Ren, H. Jiang, R. Fan, Y. Lu, Three Dimensional Printing of Bioinspired Crossed-Lamellar Metamaterials with Superior Toughness for Syntactic Foam Substitution, ACS Appl. Mater. Interfaces, 14 (2022) 42504-42512, https://doi.org/10.1021/acsami.2c12297.
[19] R.R. Paguio, A. Nikroo, M. Takagi, O. Acenas, Fabrication and overcoating of divinylbenzene foam shells using dual initiators, J. Appl. Polym. Sci., 101 (2006) 2523-2529, https://doi.org/10.1002/app.23906.
[20] M. Nollet, M. Merce, E. Laurichesse, A. Pezon, O. Soubabere, S. Besse, V. Schmitt, Water fluxes and encapsulation efficiency in double emulsions: impact of emulsification and osmotic pressure unbalance, Soft Matter, 12 (2016) 3412-3424, https://doi.org/10.1039/c5sm03089g.
[21] D. Chong, X. Liu, H. Ma, G. Huang, Y.L. Han, X. Cui, J. Yan, F. Xu, Advances in fabricating double-emulsion droplets and their biomedical applications, Microfluidics and Nanofluidics, 19 (2015) 1071-1090, https://doi.org/10.1007/s10404-015-1635-8.
[22] J. Bertling, J. Blömer, R. Kümmel, Hollow Microsperes, Chemical Engineering & Technology, 27 (2004) 829-837, https://doi.org/10.1002/ceat.200406138.
[23] A. Jaworek, Electrospray droplet sources for thin film deposition, J. Mater. Sci., 42 (2006) 266-297, https://doi.org/10.1007/s10853-006-0842-9.
[24] P. Zhu, L. Wang, Microfluidics-Enabled Soft Manufacture of Materials with Tailorable Wettability, Chem. Rev., (2021), https://doi.org/10.1021/acs.chemrev.1c00530.
[25] H. Wu, Y. Ren, T. Jiang, J. Chen, W. Wu, Y. Lu, H. Jiang, Synthesis of tubular silica fiber via all‐aqueous microfluidics for geopolymer regulation, Int. J. Appl. Ceram. Tec., (2022), https://doi.org/10.1111/ijac.14140.
[26] X. Chen, L. Hou, Z. Zhang, R. Lin, R. Lin, C. Yan, F. Bao, Microfluidic encapsulation of soluble reagents with large-scale concentration gradients in a sequence of droplets for comparative analysis, Colloids and

Surfaces A: Physicochemical and Engineering Aspects, 655 (2022) 130227, https://doi.org/10.1016/j.colsurfa.2022.130227.
[27] L. Hou, Y. Ren, W. Liu, X. Deng, X. Chen, T. Jiang, G. Wu, H. Jiang, Eccentric magnetic microcapsule for on-demand transportation, release, and evacuation in microfabrication fluidic networks, Colloids and Surfaces A: Physicochemical and Engineering Aspects, 599 (2020) 124905, https://doi.org/10.1016/j.colsurfa.2020.124905.
[28] L. Hou, Z. Liang, X. Fan, J. Yu, F. Bao, Bioinspired self-coiling Janus microfiber actuators for micro-lifter and humidity sensing, Sensors and Actuators B: Chemical, 394 (2023) 134344, https://doi.org/10.1016/j.snb.2023.134344.
[29] L.R. Arriaga, E. Amstad, D.A. Weitz, Scalable single-step microfluidic production of single-core double emulsions with ultra-thin shells, Lab Chip, 15 (2015) 3335-3340, https://doi.org/10.1039/c5lc00631g.
[30] L. Shang, Y. Cheng, J. Wang, H. Ding, F. Rong, Y. Zhao, Z. Gu, Double emulsions from a capillary array injection microfluidic device, Lab Chip, 14 (2014) 3489-3493, https://doi.org/10.1039/c4lc00698d.
[31] C.X. Zhao, D. Chen, Y. Hui, D.A. Weitz, A.P.J. Middelberg, Controlled Generation of Ultrathin-Shell Double Emulsions and Studies on Their Stability, Chemphyschem, 18 (2017) 1393-1399, https://doi.org/10.1002/cphc.201601334.
[32] C.H. Choi, D.A. Weitz, C.S. Lee, One step formation of controllable complex emulsions: from functional particles to simultaneous encapsulation of hydrophilic and hydrophobic agents into desired position, Adv. Mater., 25 (2013) 2536-2541, https://doi.org/10.1002/adma.201204657.
[33] J. Wang, S. Hahn, E. Amstad, N. Vogel, Tailored Double Emulsions Made Simple, Adv. Mater., 34 (2022) e2107338, https://doi.org/10.1002/adma.202107338.
[34] N. Teo, C. Jin, A. Kulkarni, S.C. Jana, Continuous fabrication of core-shell aerogel microparticles using microfluidic flows, J. Colloid Interface Sci., 561 (2020) 772-781, https://doi.org/10.1016/j.jcis.2019.11.053.
[35] N.N. Deng, Z.J. Meng, R. Xie, X.J. Ju, C.L. Mou, W. Wang, L.Y. Chu, Simple and cheap microfluidic devices for the preparation of monodisperse emulsions, Lab Chip, 11 (2011) 3963-3969, https://doi.org/10.1039/c1lc20629j.
[36] A. Vian, E. Amstad, Mechano-responsive microcapsules with uniform thin shells, Soft Matter, 15 (2019) 1290-1296, https://doi.org/10.1039/c8sm02047g.
[37] A.K. Tucker-Schwartz, Z. Bei, R.L. Garrell, T.B. Jones, Polymerization of electric field-centered double emulsion droplets to create polyacrylate shells, Langmuir, 26 (2010) 18606-18611, https://doi.org/10.1021/la103719z.
[38] S. Liang, J. Li, Q. Xu, J. Man, H. Chen, Hydrodynamically Formed Uniform Thick Coatings on Microspheres, Small, 14 (2018) e1800613, https://doi.org/10.1002/smll.201800613.
[39] H. Sameh, E. Wafa, B. Sihem, L.C. Fernando, Influence of diffusive transport on the structural evolution of W/O/W emulsions, Langmuir, 28 (2012) 17597-17608, https://doi.org/10.1021/la303469j.
[40] J. Bahtz, D.Z. Gunes, E. Hughes, L. Pokorny, F. Riesch, A. Syrbe, P. Fischer, E.J. Windhab, Decoupling of mass transport mechanisms in the stagewise swelling of multiple emulsions, Langmuir, 31 (2015) 5265-5273, https://doi.org/10.1021/acs.langmuir.5b01138.
[41] J. Bahtz, D.Z. Gunes, A. Syrbe, N. Mosca, P. Fischer, E.J. Windhab, Quantification of Spontaneous W/O Emulsification and its Impact on the Swelling Kinetics of Multiple W/O/W Emulsions, Langmuir, 32 (2016) 5787-5795, https://doi.org/10.1021/acs.langmuir.6b00425.
[42] F. Tu, D. Lee, Controlling the stability and size of double-emulsion-templated poly(lactic-co-glycolic)

acid microcapsules, Langmuir, 28 (2012) 9944-9952, https://doi.org/10.1021/la301498f.
[43] B. Khadem, M. Khellaf, N. Sheibat-Othman, Investigating swelling-breakdown in double emulsions, Colloids and Surfaces A: Physicochemical and Engineering Aspects, 585 (2020) 124181, https://doi.org/10.1016/j.colsurfa.2019.124181.
[44] W. Zhang, L. Qu, H. Pei, Z. Qin, J. Didier, Z. Wu, F. Bobe, D.E. Ingber, D.A. Weitz, Controllable Fabrication of Inhomogeneous Microcapsules for Triggered Release by Osmotic Pressure, Small, 15 (2019) e1903087, https://doi.org/10.1002/smll.201903087.
[45] W. Zhang, A. Abbaspourrad, D. Chen, E. Campbell, H. Zhao, Y. Li, Q. Li, D.A. Weitz, Osmotic Pressure Triggered Rapid Release of Encapsulated Enzymes with Enhanced Activity, Adv. Funct. Mater., 27 (2017) 1700975, https://doi.org/10.1002/adfm.201700975.
[46] L. Shang, Y. Cheng, J. Wang, Y. Yu, Y. Zhao, Y. Chen, Z. Gu, Osmotic pressure-triggered cavitation in microcapsules, Lab Chip, 16 (2016) 251-255, https://doi.org/10.1039/c5lc01286d.
[47] D.M. El-Sherif, M.A. Wheatley, Development of a novel method for synthesis of a polymeric ultrasound contrast agent, J Biomed Mater Res A, 66 (2003) 347-355, https://doi.org/10.1002/jbm.a.10586.
[48] Y.H. Kim, D.J. Kim, S. Lee, D.H. Kim, S.G. Park, S.H. Kim, Microfluidic Designing Microgels Containing Highly Concentrated Gold Nanoparticles for SERS Analysis of Complex Fluids, Small, 15 (2019) e1905076, https://doi.org/10.1002/smll.201905076.
[49] S. Zhuang, H. Liu, D.W. Inglis, M. Li, Tuneable Cell-Laden Double-Emulsion Droplets for Enhanced Signal Detection, Anal. Chem., (2023), https://doi.org/10.1021/acs.analchem.2c04697.
[50] S.H. Kim, J.G. Park, T.M. Choi, V.N. Manoharan, D.A. Weitz, Osmotic-pressure-controlled concentration of colloidal particles in thin-shelled capsules, Nat Commun, 5 (2014) 3068, https://doi.org/10.1038/ncomms4068.
[51] T.M. Choi, J.-G. Park, Y.-S. Kim, V.N. Manoharan, S.-H. Kim, Osmotic-Pressure-Mediated Control of Structural Colors of Photonic Capsules, Chem. Mater., 27 (2015) 1014-1020, https://doi.org/10.1021/cm5043292.
[52] L. Hou, Y. Ren, Y. Jia, X. Chen, X. Deng, Z. Tang, Q. Hu, Y. Tao, H. Jiang, Osmolarity-controlled swelling behaviors of dual-cored double-emulsion drops, Microfluidics and Nanofluidics, 21 (2017), https://doi.org/10.1007/s10404-017-1897-4.
[53] X. Guan, L. Hou, Y. Ren, X. Deng, Q. Lang, Y. Jia, Q. Hu, Y. Tao, J. Liu, H. Jiang, A dual-core double emulsion platform for osmolarity-controlled microreactor triggered by coalescence of encapsulated droplets, Biomicrofluidics, 10 (2016) 034111, https://doi.org/10.1063/1.4952572.
[54] H. Wu, Y. Ren, T. Jiang, W. Wu, Y. Lu, H. Jiang, Fabrication of syntactic foam fillers via integrated on/off-chip microfluidic methods for optimized geopolymer composites, Lab Chip, (2022), https://doi.org/10.1039/d1lc00901j.
[55] X. Deng, Y. Ren, L. Hou, T. Jiang, H. Jiang, Continuous microfluidic fabrication of anisotropic microparticles for enhanced wastewater purification, Lab Chip, 21 (2021) 1517-1526, https://doi.org/10.1039/d0lc01298j.
[56] A.S. Utada, A. Fernandez-Nieves, H.A. Stone, D.A. Weitz, Dripping to jetting transitions in coflowing liquid streams, Phys. Rev. Lett., 99 (2007) 094502, https://doi.org/10.1103/PhysRevLett.99.094502.
[57] A. Montessori, M. Lauricella, E. Stolovicki, D.A. Weitz, S. Succi, Jetting to dripping transition: Critical aspect ratio in step emulsifiers, Physics of Fluids, 31 (2019) 021703, https://doi.org/10.1063/1.5084797.

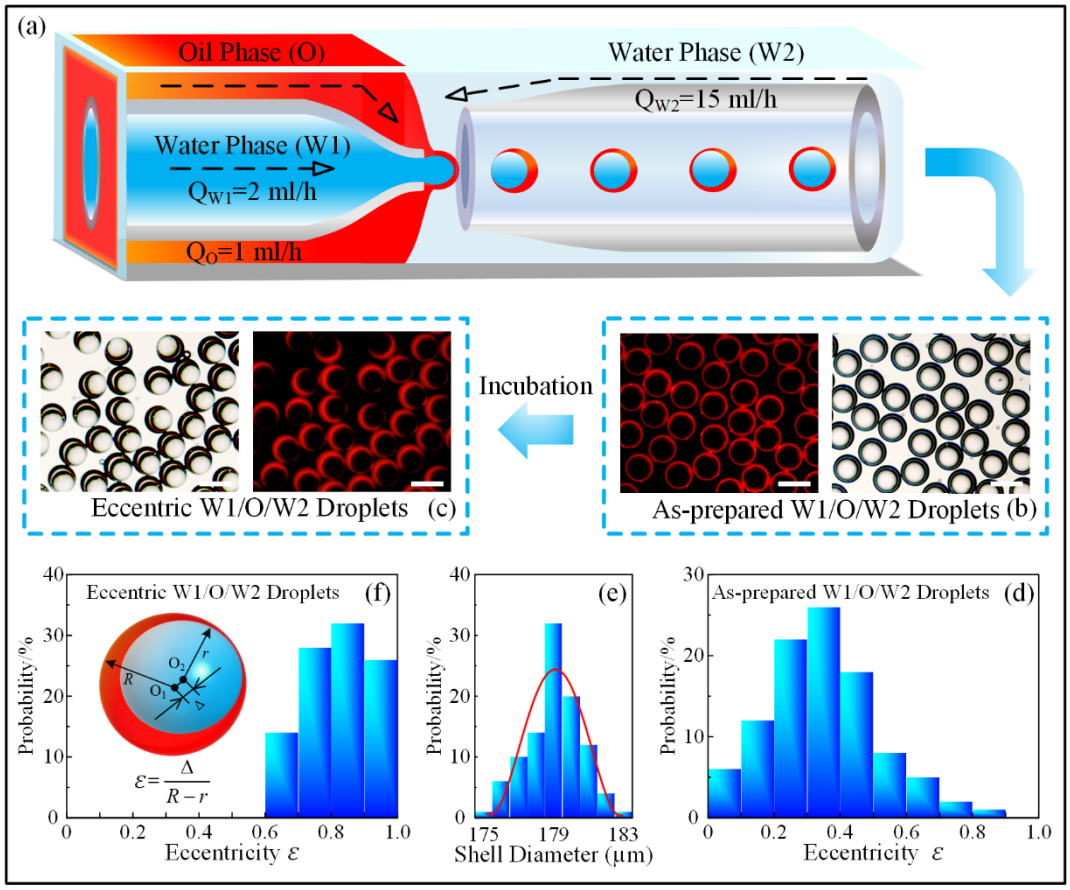

Fig. 1. Microfluidic generation of W1/O/W2 double emulsion droplets with their morphology transition from nonconcentric to fully eccentric during incubation. (a) Schematic illustration of the microfluidic generation process of W1/O/W2 double emulsion droplets using a capillary microfluidic device. (b) The optical and fluorescent images of the as-prepared W1/O/W2 double emulsion droplets, the scale bars are 200 μm. (c) The optical and fluorescent images of the same batch of W1/O/W2 double emulsion droplets after incubation, the scale bars are 200 μm. (d) Statistical analysis of the eccentricity of the as-prepared W1/O/W2 double emulsion droplets. (e) Statistical analysis of the shell diameter of the W1/O/W2 double emulsion droplets. (f) Statistical analysis of the eccentricity of the W1/O/W2 double emulsion droplets according to (c).

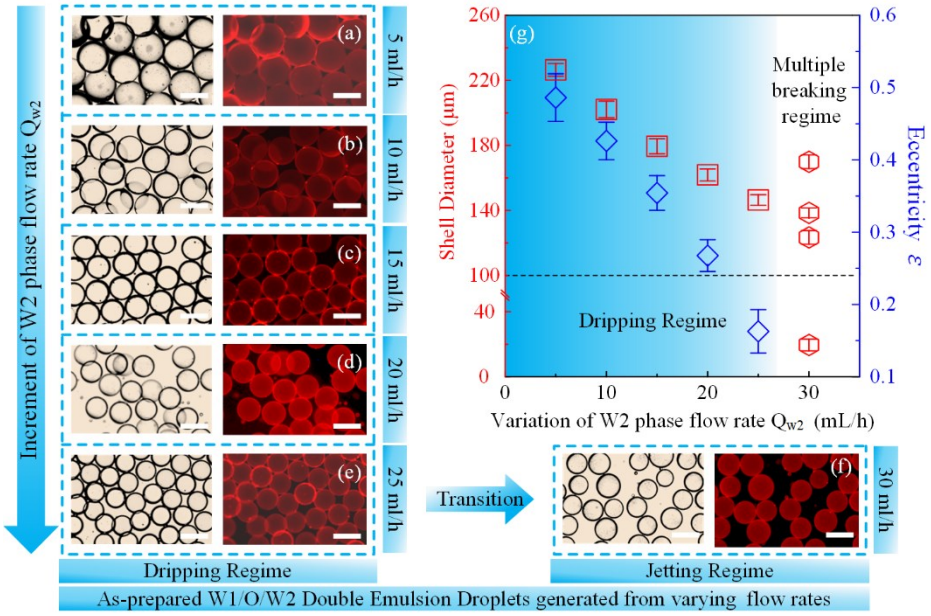

Fig. 2. Real-time hydrodynamic centering of W1/O/W2 double emulsion droplets by regulating the outer phase flow rate during the microfluidic generation process, while the flow rates of the inner and middle phases are fixed at Qw1= 2 ml/h, and Qo= 1 ml/h, respectively. (a) The optical and fluorescent images of the as-prepared monodispersed W1/O/W2 double emulsion droplets with the outer phase flow rate set to Qw2= 5 ml/h. (b) The optical and fluorescent images of the as-prepared monodispersed W1/O/W2 double emulsion droplets with the outer phase flow rate set to Qw2= 10 ml/h. (c) The optical and fluorescent images of the as-prepared monodispersed W1/O/W2 double emulsion droplets with the outer phase flow rate set to Qw2= 15 ml/h. (d) The optical and fluorescent images of the as-prepared monodispersed W1/O/W2 double emulsion droplets with the outer phase flow rate set to Qw2= 20 ml/h. (e) The optical and fluorescent images of the as-prepared monodispersed W1/O/W2 double emulsion droplets with the outer phase flow rate set to Qw2= 25 ml/h. (f) The optical and fluorescent images of the as-prepared polydispersed W1/O/W2 double emulsion droplets with the outer phase flow rate set to Qw2= 30 ml/h. (g) Relationships between the shell diameter, and the eccentricity of the W1/O/W2 double emulsion droplets with respect to the varying outer phase flow rates. The scale bars are 200 μm.

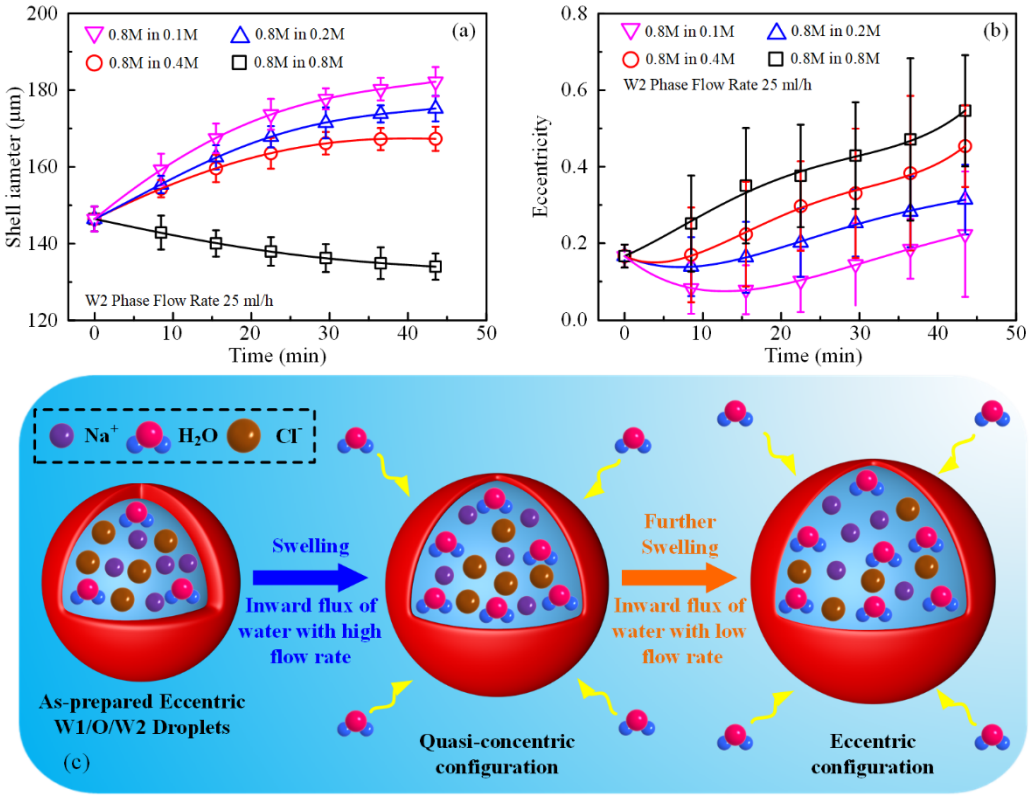

Fig. 3. Further hydrodynamic regulation of W1/O/W2 double emulsion droplets, generated by three-phase flow rates of Qw1= 2 ml/h, Qo= 1 ml/h, and Qw2= 25 ml/h, by osmotic gradient induced transmembrane water transport. (a) Shell diameter variation of the W1/O/W2 double emulsion droplets during the gradient osmosis-induced hydrodynamic regulation process. (b) Eccentricity variation of the W1/O/W2 double emulsion droplets during the gradient osmosisinduced hydrodynamic regulation process. (c) Schematic illustration of the osmosis-induced hydrodynamic regulation process.

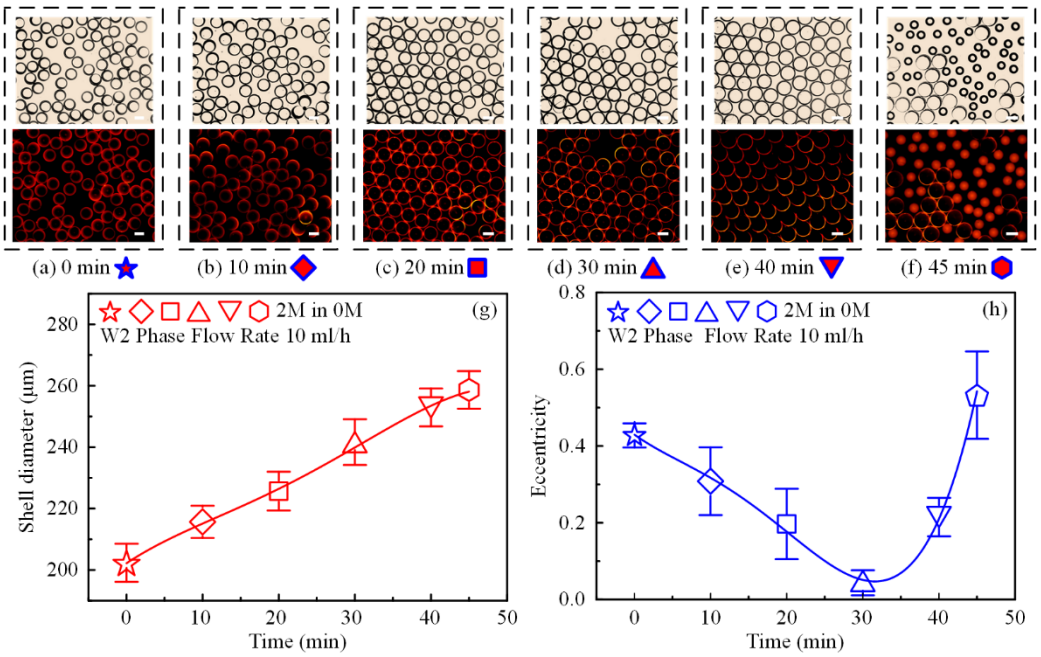

Fig. 4. Higher osmosis-induced hydrodynamic regulation process of nonconcentric W1/O/W2 double emulsion droplets generated by three-phase flow rates of Qw1= 2 ml/h, Qo= 1 ml/h, and Qw2= 10 ml/h. (a-f) The optical and fluorescent images of W1/O/W2 double emulsion droplets at different time nodes during the osmosis-induced hydrodynamic regulation process. (g) Shell diameter variation of the W1/O/W2 double emulsion droplets during the osmosis-induced hydrodynamic regulation process. (h) Eccentricity variation of the W1/O/W2 double emulsion droplets during the osmosis-induced hydrodynamic regulation process. The scale bars are 200 μm.

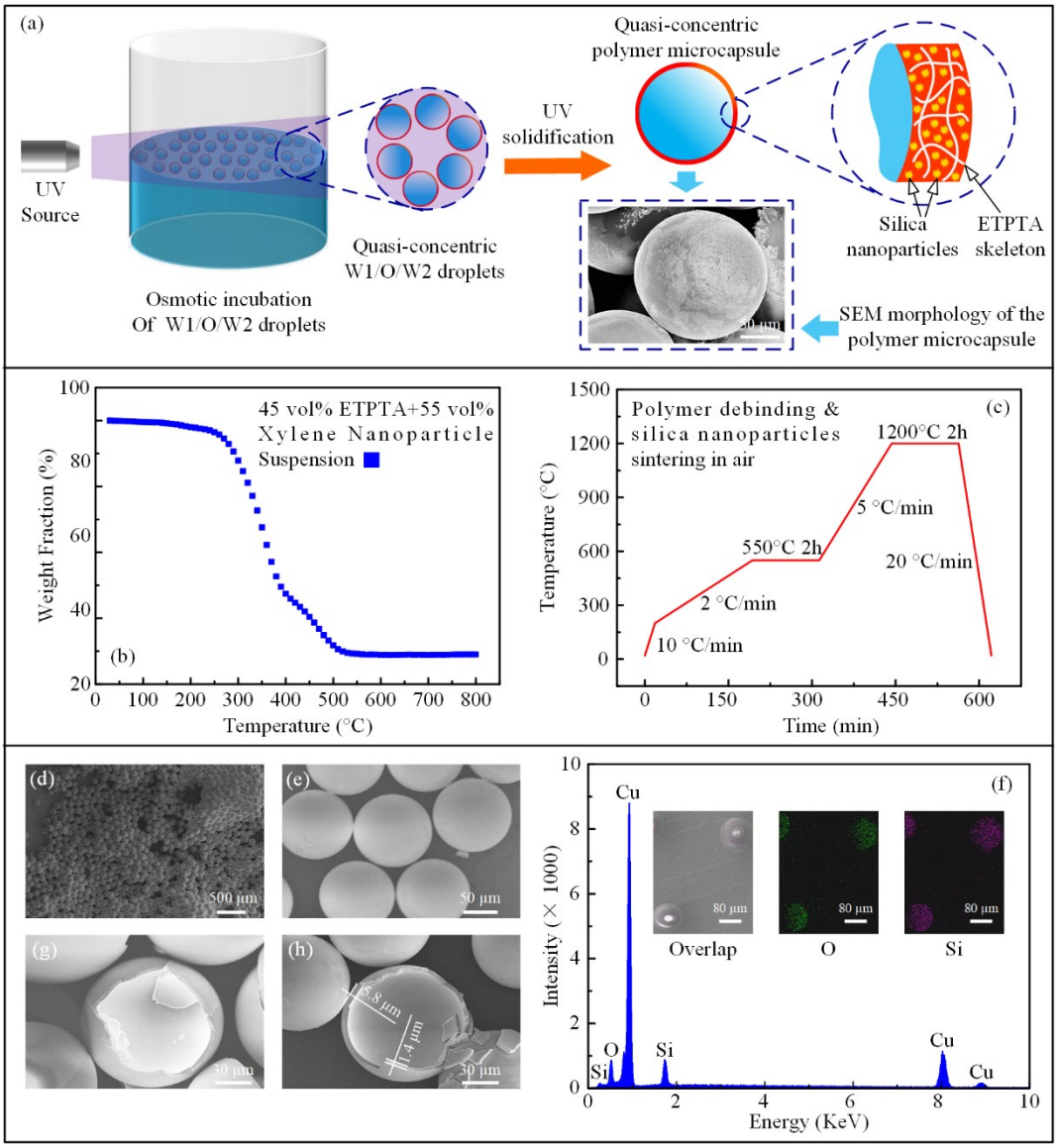

Fig. 5. Preparation of quasi-concentric polymer microcapsules and the derived ceramic microspheres. (a) Schematic illustration of the fabrication process of the quasi-concentric microcapsules based on the instant UV polymerization of the W1/O/W2 double emulsion droplets. (b) Thermogravimetric profile of the quasiconcentric polymer microcapsule. (c) One-step heat treatment curve of the polymer microcapsule including debinding and sintering in air. (d-e) SEM images of the as-prepared ceramic microspheres. (f) EDS elemental analysis result of the ceramic microspheres placed on the copper substrate. (g) SEM image of damaged quasi-concentric silica microspheres after osmosis-induced hydrodynamic regulation corresponding to the optimal configuration of droplets as marked by the pink triangle in Fig. 3b. (h) SEM image of damaged silica microspheres without osmosis-induced hydrodynamic regulation corresponding to the pink triangle group in Fig. 3b.